The Astronomical Journal, 148:56 (9pp), 2014 September doi:10.1088/0004-6256/148/3/56

DYNAMICAL IMPLANTATION OF OBJECTS IN THE KUIPER BELT

P. I. O. Brasil[1,2], D. Nesvorný[2], and R. S. Gomes[2,3]
[1] Instituto Nacional de Pesquisas Espaciais (INPE), ETE/DMC, Av. dos Astronautas, 1758, São José dos Campos, Brazil; pedro_brasil87@hotmail.com
[2] Department of Space Studies, Southwest Research Institute, 1050 Walnut Street, Boulder, CO, USA; davidn@boulder.swri.edu
[3] Observatório Nacional (ON), GPA, Rua General José Cristino, 77, Rio de Janeiro, Brazil; rodney@on.br
Received 2014 January 13; accepted 2014 June 21; published 2014 August 18

ABSTRACT

Several models have been suggested in the past to describe the dynamical formation of hot Kuiper Belt objects (hereafter Hot Classicals or HCs for short). Here, we discuss a dynamical mechanism that allows orbits to evolve from the primordial planetesimal disk at $\lesssim$35 AU to reach the orbital region now occupied by HCs. We performed three different sets of numerical simulations to illustrate this mechanism. Two of these simulations were based on modern theories for the early evolution of the solar system (the Nice and jumping-Jupiter models). The third simulation was performed with the purpose of increasing the resolution at 41–46 AU. The common aspect of these simulations is that Neptune scatters planetesimals from $\lesssim$35 AU to >40 AU and then undergoes a long phase of slow residual migration. Our results show that to reach an HC orbit, a scattered planetesimal needs to be captured in a mean motion resonance (MMR) with Neptune where the perihelion distance rises due to the Kozai resonance (which occurs in MMRs even for moderate inclinations). Finally, while Neptune is still migrating, the planetesimal is released from the MMR on a stable HC orbit. We show that the orbital distribution of HCs expected from this process provides a reasonable match to observations. The capture efficiency and the mass deposited into the HC region appears to be sensitive to the maximum eccentricity reached by Neptune during the planetary instability phase. Additional work will be needed to resolve this dependency in detail.

Key words: Kuiper belt: general – planetary systems

Online-only material: color figure

1. INTRODUCTION

Since the early 1990s a whole new field of solar system research has emerged which deals with trans-Neptunian objects (TNOs). Although the trans-Neptunian region had been studied before from a theoretical point of view (Edgeworth 1949; Kuiper 1951, 1974), the turning point was the discovery of $1992\,QB_1$ by Jewitt & Luu (1993). Hundreds of discoveries have been made since then. Now, 567 TNOs have been observed in more than one opposition.[4]

According to orbital properties, the trans-Neptunian region can be divided into at least four populations (Jewitt et al. 1998; Gladman et al. 2002; Gomes et al. 2005b, 2008). These populations are as follows.

1. Classical Kuiper Belt composed of non-resonant bodies with a semi-major axis of 39.4 AU $\leqslant a \leqslant$ 48 AU. It is possible to subdivide this population into Cold Classicals (CCs; $i < 5^\circ$) and Hot Classicals (HCs; $i > 5^\circ$ with inclinations up to 30°; Brown 2001).
2. Resonant objects trapped in exterior mean motion resonances (MMRs) with Neptune, mainly the 2:3, 1:2, and 2:5 MMRs. The 2:3 MMR population is also known as Plutinos, after its largest member Pluto.
3. Scattered disk objects usually classified as those with a perihelion distance of 30 AU $\lesssim q <$ 35 AU and a semi-major axis of $a >$ 50 AU. The scattered disk is thought to be the main source of the Jupiter-family comets (Duncan & Levison 1997).
4. Extended scattered disk, whose members are also sometimes called the detached objects. The detached objects have $a >$ 50 AU and $q \geqslant$ 40 AU, which places them in the region where they do not have close encounters with Neptune. Their orbits are therefore stable on long timescales. Only 13 detached objects are currently known due to the difficulty of detecting them observationally.

This complex dynamical structure of the Kuiper Belt was largely unexpected because the formation of these bodies must have occurred in a dynamically cold disk (Kenyon & Luu 1999).

Various theories have been developed to explain the different dynamical populations in the Kuiper Belt. To explain the resonant objects, the "sweeping resonance mechanism" was proposed by Malhotra (1993, 1995, 1998). These works mainly aimed to explain the peculiar orbits of the Plutinos locked in the 2:3 MMR with Neptune. They showed that bodies are trapped in resonances with Neptune during Neptune's outward migration (Fernandez & Ip 1984). This process, with Neptune's migration into a dynamically cold disk, is able to reproduce the distribution of orbital eccentricities of Plutinos but it cannot explain their sometimes large orbital inclinations (Gomes 2000). Hahn & Malhotra (2005) therefore considered models in which Neptune migrates into a dynamically excited disk.

The dynamical origin of the classical Kuiper Belt objects is more of a puzzle. For example, Morbidelli & Valsecchi (1997) and Petit et al. (1999) proposed that HCs could have arrived in their orbits due to the long-term presence of a massive object which would excite their primordial orbits. This model, however, is unable to explain the inclination distribution of HCs that extends up to 30°, because a massive object could not produce such large inclinations. Levison & Morbidelli (2003) argued that CCs were delivered to their present orbits by sweeping 1:2 MMR with Neptune while Neptune was migrating. For this to work, Neptune has to migrate from an orbit such that its exterior 1:2 resonance is initially located inside the planetesimal disk. More recent formation theories of the classical Kuiper Belt consider planetary migration scenarios in

[4] http://www.minorplanetcenter.net/iau/lists/TNOs.html—as of 2013 August 22.

which Neptune is first scattered out during dynamical instability in the outer system (see below), and then migrates out.

Two varieties of instability models currently exist. The first is the original Nice model (Tsiganis et al. 2005; Gomes et al. 2005a; Morbidelli et al. 2005), in which the instability is triggered when Jupiter and Saturn migrate past their 2:1 resonance. This excites planetary orbits such that encounters of Saturn with Uranus and/or Neptune occur. The Nice model successfully explains the current giant planet orbits, the Late Heavy Bombardment of the Moon, capture of Jupiter Trojans, etc. The second variety, which is the instability model currently favored, is the jumping-Jupiter scenario. This is a modification of the Nice model which requires that Jupiter's orbits suffered discontinuous changes due to encounters with Uranus or Neptune. This mode of evolution is required from constraints from the secular architecture of the outer planetary system, the survival of the terrestrial planets, and the dynamical structure of the asteroid belt (Morbidelli et al. 2009, 2010; Brasser et al. 2009). Recent works suggested that the jumping-Jupiter models can conveniently be obtained if the early solar system contained an extra ice giant that was presumably ejected into interstellar space during the instability (Nesvorný 2011; Nesvorný & Morbidelli 2012; Batygin et al. 2012).

Levison et al. (2008), inspired by the original Nice model, reenacted Neptune's migration phase starting from an eccentric orbit ($e_{\rm N} \simeq 0.3$). They assumed that Neptune's orbital eccentricity decreases over a characteristic damping timescale of $\tau_e = 1$ Myr. At the same time, Neptune was assumed to migrate from $\simeq$28 AU to 30 AU on a characteristic migration timescale of $\tau_a = 1$ Myr. Both CCs and HCs were captured during the initial phase of Neptune's orbital evolution when, according to Levison et al. (2008), the exterior MMRs overlapped and created a global region of chaotic orbits ("chaotic sea"). The bodies previously scattered to $a > 40$ AU by Neptune thus wandered into this chaotic sea, the eccentricities decreased, and the bodies were permanently captured into the classical belt when Neptune's eccentricity dropped.

A potential problem with the common origin of CCs and HCs in the model of Levison et al. (2008) is their differences in physical properties such as color, size frequency distribution, albedo, and binary fraction (Levison & Stern 2001; Bernstein et al. 2004; Fraser et al. 2014; Parker & Kavelaars 2010). These differences would be difficult to explain if CCs and HCs started at the same location in the transplanetary disk. Moreover, Dawson & Murray-Clay (2012) pointed out that the chaotic sea of Levison et al. (2008) does not, in fact, exist even if $e_{\rm N} \sim 0.3$. This raises a question of how, in reality, the current orbits of the HCs and CCs were reached.

As for CCs, given their different properties mentioned above, the most straightforward method is to assume that they formed in situ (Batygin et al. 2011). As for HCs, Dawson & Murray-Clay (2012) suggested that their capture can occur from purely secular interactions between an eccentric Neptune and bodies in the scattered disk. This interaction produces large oscillations of eccentricity, and therefore of the perihelion distance of scattered bodies, a fraction of which can decouple from Neptune when Neptune's eccentricity drops.

In light of the above uncertainties, we decided to study the dynamical origin of the classical belt by considering three different migration/instability models (Models A, B, and C). Model A features a phase when Neptune is scattered on to a highly eccentric orbit. This case is therefore similar to those considered in Levison et al. (2008). In Model B, taken from Nesvorný & Morbidelli (2012), Neptune's eccentricity never becomes very large. Model C, which was designed with particular focus on HCs, has an improved resolution in the region between 41 and 46 AU. This model was built in a more artificial way to mimic the fate of scattered particles generated in Models A and B.

We show that HCs form by a specific dynamical pathway in all of these models, where Kozai oscillations inside the MMRs and slow residual migration of Neptune play important roles. This mechanism is similar to one of the dynamical mechanisms first pointed out in Gomes (2003a, 2003b). Here, we perform a comprehensive analysis of this mechanism and show its relevance in the currently favored models for the early evolution of the solar system.

2. MODEL A: HIGH ECCENTRICITY OF NEPTUNE

Initially, we set up a system with the Sun, the four major planets and an outer disk of planetesimals. The terrestrial planet masses were added to the mass of the Sun. The initial orbital semi-major axes were 5.45 AU, 8.18 AU, 12.0 AU, and 14.2 AU for Jupiter, Saturn, Uranus, and Neptune, respectively. Their eccentricities were initially zero and their inclinations were $\leqslant 0.^\circ 5$. The planetesimal disk was initially composed of 600 bodies with a total mass of 42 $M_{\rm Earth}$. Planetesimals had initially zero eccentricities and inclinations. The planetesimal disk had a surface density proportional to r^{-1}, where r is the heliocentric distance, and was located between 16 AU and 40 AU. These initial conditions are based on the original Nice model (Tsiganis et al. 2005; Gomes et al. 2005a; Morbidelli et al. 2005) where we basically aimed to generate the onset of the planetary instability phase at around the right time and with the planetary orbits parked on final orbits similar to their present ones. However, our model includes jumping-Jupiter close encounters of an ice giant with Jupiter. It must be noted that in the original scenario, the instability was triggered by the slow approach of Jupiter and Saturn to their mutual 1:2 MMR. This kind of evolution was later found to lead to destructive instabilities to the inner planetary system as well as to produce an orbital distribution of the asteroid belt inconsistent with the actual one (Morbidelli et al. 2009, 2010; Brasser et al. 2009). However, we found that just after the onset of planetary instability, the original Nice model does not fundamentally differ from its more recent reincarnations, which justifies our use of it here to determine its consequences for the hot Kuiper Belt. The numerical integration of the equations of motion was performed with the hybrid version of the `Mercury` integrator (Chambers 1999), using a step length of 0.5 yr.

Neptune stops not much beyond 30 AU in this simulation because the planetesimal disk beyond 30 AU is scattered during the instability, which reduces its power to sustain migration. Figure 1 shows the orbital evolution of Neptune in the simulation. The scattering event occurred at $t \simeq 6.5 \times 10^8$ yr and generated $e_{\rm N} \simeq 0.4$. The eccentricity then dropped back to near zero over the next 5 Myr. When the stage of mutual encounters between planets was over, we cloned each planetesimal 100 times to obtain better statistics. The cloning was done by distributing the mass of the initial disk particle among 100 new particles with slightly different velocities. The cloning therefore preserves the total disk mass.

By analyzing the results, we find that 50 disk particles ended with orbits compatible with those of HCs, with $i > 5^\circ$, $q > 30$ AU, and 40 AU $< a <$ 47.5 AU (i.e., only including orbits between the 2:3 and 1:2 MMRs with Neptune) in Figure 2.

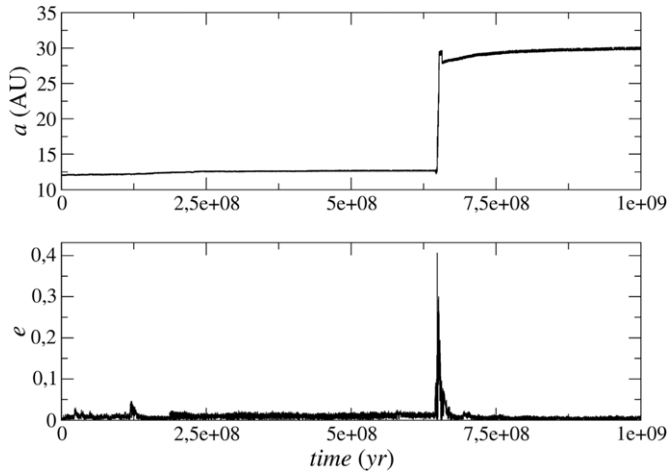

Figure 1. Evolution of Neptune's orbit in our Model A simulation. The upper panel shows the semi-major axis of Neptune and the bottom panel shows its eccentricity for a time interval of 1 Gyr. The complete integration was 4.5 Gyr, but the instability event occurs at ≃650 Myr.

This figure shows that there is good agreement between the orbital distribution of simulated and real HCs. The eccentricity distribution of simulated HCs extends from around 0.3 to fairly small eccentricities near 0.04, with some ending with $q > 45$ AU, just as needed. Note that these orbits are the most difficult to produce from the original disk because a robust mechanism is needed to implant orbits so deeply into the HC region. Also, the inclinations of HC particles extend all the way above ≃25°, just as needed to explain the high i component of real HCs. We caution, however, that a detailed comparison would require us to account for observational biases. In Figure 2, we note a gap in the distribution of the simulated HCs between the 5:9 and 7:13 MMRs which does not exist in the real distribution. We would expect that objects could be captured into the 6:11 and 7:13 MMRs and be released from them to fill this gap. However, these resonances may be too weak for any efficient capture probability. On the other hand, HCs populating this region might have been released from the 1:2 MMR if the extension of Neptune's residual migration was large enough.

We analyzed the orbital evolution of individual particles to determine the mechanism by which they reach the HC orbits. We found that many of our HCs are planetesimals that were first scattered by Neptune and then trapped in some MMR with Neptune, such as the 1:2 or 5:9 MMRs. While inside the MMR, they experienced the effects of the Kozai resonance (Kozai 1962, 1985; Gallardo et al. 2012), which leads to large anti-correlated oscillations of eccentricity and inclination. In some cases, while Neptune is still migrating, the particle can fall off from the MMRs during a stage when its eccentricity is near its minimum. Once this happen, the orbit of the particle stabilizes in the HC region.

Figure 3 shows an example of a particle that was scattered by Neptune and was subsequently trapped in the 1:2 MMR with Neptune (see the top left and bottom right panels). The particle remains in the 1:2 MMR with Neptune up to 790 Myr. The Kozai resonance is active between ∼700–715 Myr and between ∼730–780 Myr (see the libration of the argument of perihelion around 90° in the top right panel). This causes a high variation of the perihelion distance. These variations happen while the particle is in 1:2 MMR. When the MMR resonance is broken, at ∼800 Myr, the particle is released into an HC orbit where it stays for the rest of the simulation. The final semi-major axis is $a = 46.5$ AU and the orbital inclination is $i \sim 26°$.

Figure 4 shows another example. Now, after being scattered, the object evolves very close to 5:9 MMR, and is eventually captured by this resonance at ∼780 Myr. It then experiences slow variation of its argument of perihelion, which is a sign that the orbit evolves near the separatrix of the Kozai resonance, allowing it to reach large values of perihelion distance and inclination. The MMR is broken at ∼900 Myr (bottom right panel), after the particle passes through a phase in which its perihelion distance remains large for a long period of time. After

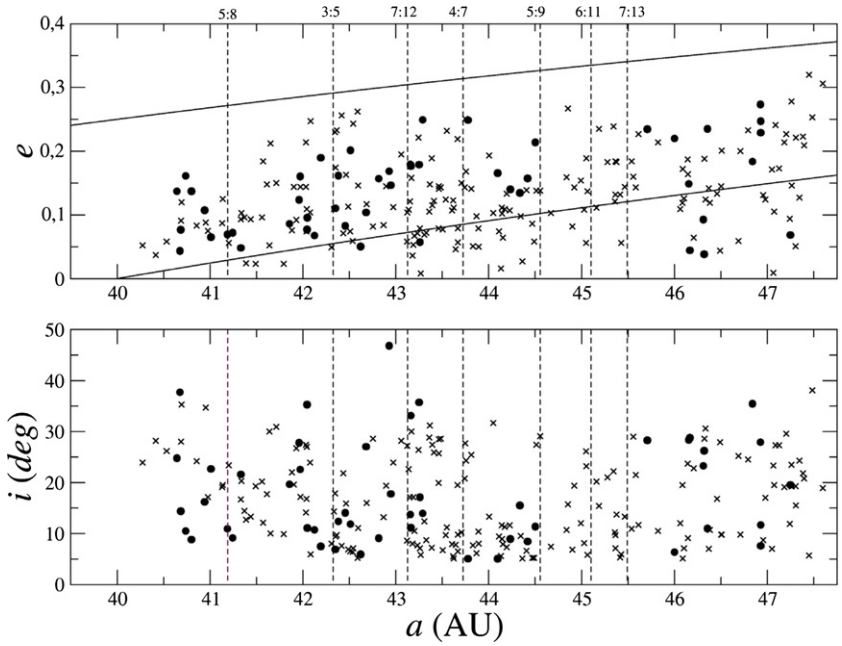

Figure 2. Semi-major axis vs. eccentricity (top) and semi-major axis vs. inclination (bottom) distribution of the particles with $i > 5°$. These particles were captured and survived in Model A in the region of the hot classical Kuiper Belt. The filled circles are the simulated objects, while the crosses are the real HCs observed for three or more oppositions. The curves in the top panel show $q = 40$ AU and $q = 30$ AU for reference. The vertical dashed lines show several MMRs in the semi-major axis interval of the classical Kuiper Belt.

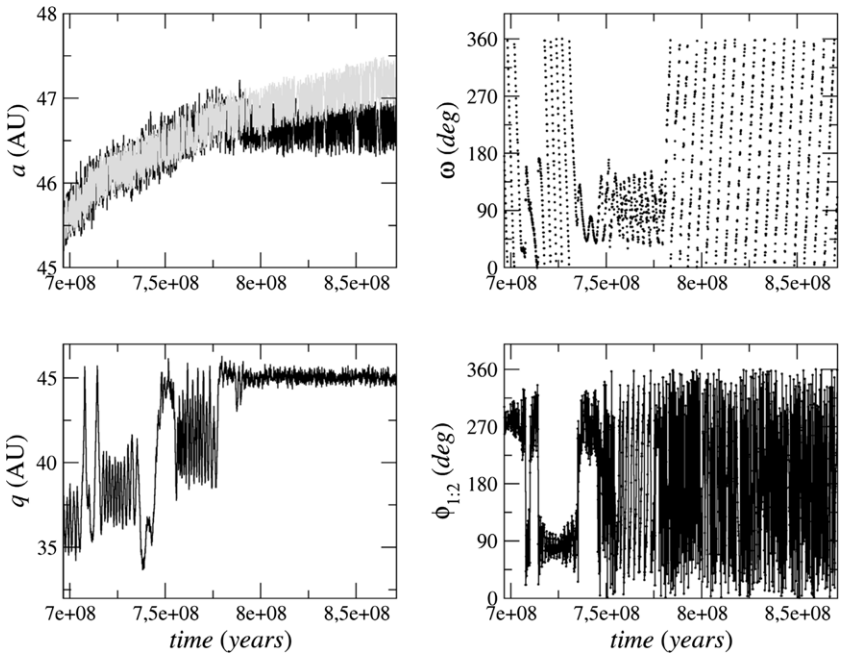

Figure 3. Orbital evolution of a particle from Model A. We show the semi-major axis of the particle (black) and the semi-major axis of Neptune's 1:2 MMR (gray) in top left panel, perihelion distance in bottom left panel, argument of perihelion, ω, in top right panel, and 1:2 MMR angle in the bottom right panel. The particle ends up on an HC orbit with $q \simeq 45$ AU after being released from the 1:2 MMR resonance.

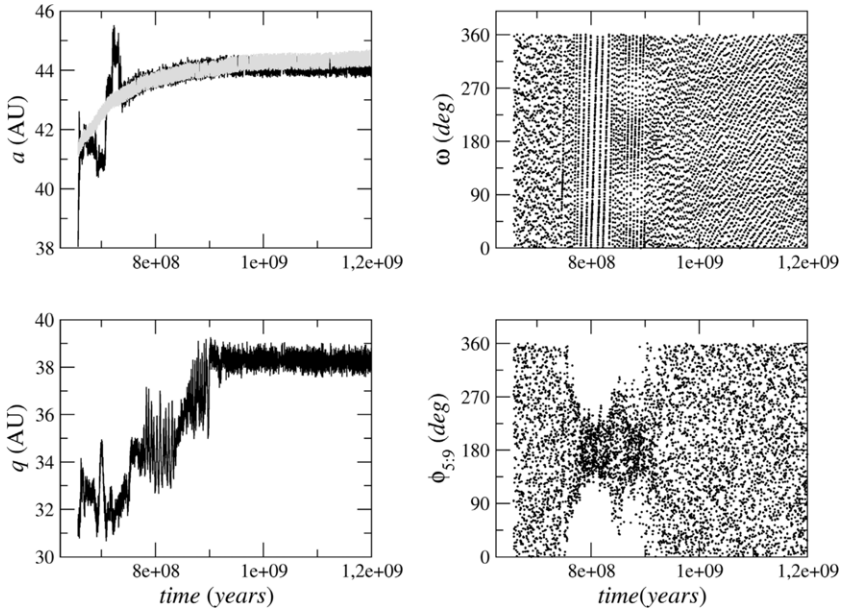

Figure 4. Same as Figure 3, but for a particle that becomes captured in the 5:9 MMR with Neptune. The particle is released from the MMR on a stable HC orbit with $q \simeq 38$ AU.

that, the object is released in a stable HC orbit with $a \simeq 44$ AU, $i \simeq 16^\circ$, and $e \simeq 0.135$.

We find that most test particles that ended in the HC region in our simulation evolved to their final orbits through the mechanism described and illustrated above. This mechanism is reminiscent of, but involving different MMRs from, that proposed by Gomes (2011) and Brasil et al. (2014) for the dynamical origin of detached objects (e.g., $2004XR_{190}$). Previously, Gomes (2000) discussed capture into MMRs and the effects of the Kozai resonance, in the context of capture of Plutinos from the scattered disk. Moreover, Gomes (2003a, 2003b) presented a general discussion of this mechanism for smooth migration histories of Neptune. Here, we show that this mechanism is general and occurs in the Nice-type instability model.

3. MODEL B: LOW ECCENTRICITY OF NEPTUNE

Dawson & Murray-Clay (2012) discussed constraints from the HCs and CCs on the migration history of Neptune. The CC constraint requires that the eccentricity of Neptune was either never really large ($e \lesssim 0.1$) or that it was large but was quickly damped by the dynamical friction from the planetesimal disk. For example, the simulation discussed in the previous section would formally violate this constraint because Neptune's

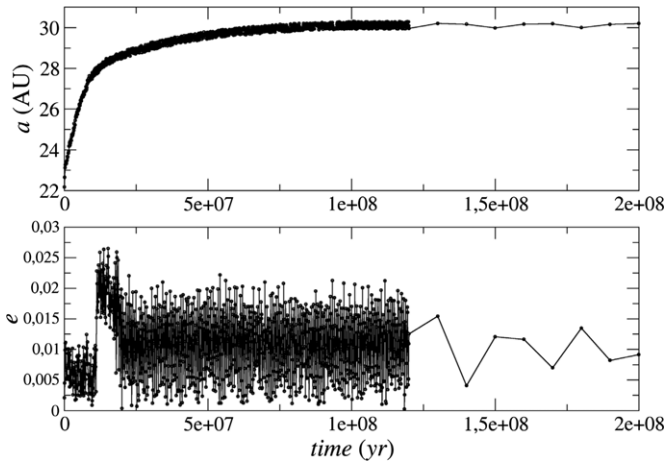

Figure 5. Evolution of Neptune's orbit in our Model B simulation. The upper panel shows the semi-major axis of Neptune from the instability near $t = 0$ up to $t = 10^9$ yr (the actual simulation was run up to 4 Gyr after the instability). The bottom panel shows Neptune's eccentricity for the same interval. Note that the sampling of orbital elements changed at 120 Myr.

eccentricity remains relatively high ($e > 0.1$) for $\simeq$5 Myr, while Neptune's semi-major axis is at $\simeq$28 AU. It is therefore desirable to consider migration models that are more in line with the findings of Dawson & Murray-Clay (2012).

To investigate this possibility, we have selected a representative case from the work of Nesvorný & Morbidelli (2012). These authors performed nearly 10^4 numerical integrations of planetary instability, starting from hundreds of different initial configurations of planets which were obtained from previous hydrodynamical and *N*-body calculations. The integrations included the effects of the transplanetary planetesimal disk. Here, we considered a case with five initial planets from this work, where the additional planet was placed onto a resonant orbit between Saturn and the inner ice giant. This is because, as shown in Nesvorný & Morbidelli (2012), including extra planets helps to boost the success rate of the instability simulations, since planets can readily be ejected into interstellar space during the instability.

In the specific run considered here, the initial orbital semi-major axes for the planets were 5.47, 7.46, 10.11, 17.58, and 22.17 AU for Jupiter, Saturn, third ice giant, Uranus, and Neptune, respectively. The third ice giant was given a mass equal to that of Neptune. The planetesimal disk was initially composed of 3000 massive bodies with the total mass of 20 $M_{\rm Earth}$. Planetesimals initially had zero eccentricities and inclinations. The planetesimal disk was located between 23 AU and 30 AU. This setup was motivated by some of the most successful models of dynamical instability in the outer solar system developed in Nesvorný & Morbidelli (2012) (see the Appendix for a discussion of these models). We used a slightly larger semi-major axis of Uranus than Nesvorný & Morbidelli (2012), such that Uranus and Neptune did not end up migrating past their 2:1 resonance. This allowed us to more easily select the instability models which are applicable to the Kuiper Belt.

Figure 5 shows the orbital evolution of Neptune in the simulation. The instability was triggered in this simulation when planetesimals, scattered by migrating Neptune from the outer disk, evolved into the Jupiter-Saturn region. As a result of the gravitational interaction with planetesimals, Saturn migrated outward and destabilized the orbit of the neighboring ice giant. The phase of scattering between the ice giant and Jupiter/Saturn occurred $t \simeq 10^7$ yr after the start of the simulation

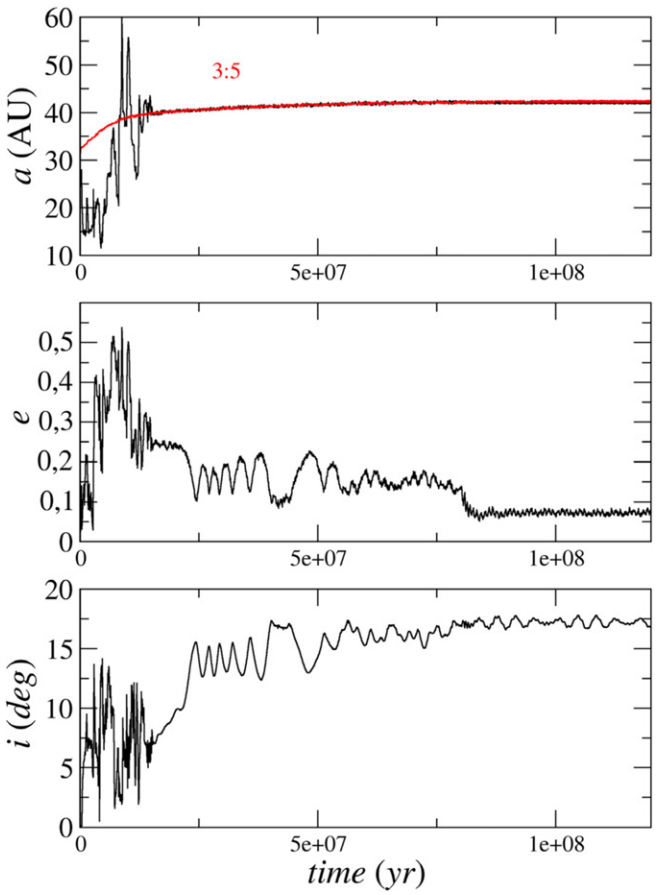

Figure 6. Semi-major axis, eccentricity, and inclination of a disk particle that reached an HC orbit in our simulations of Model B. The red line in the upper panel shows the semi-major axis location of the 3:5 MMR with Neptune.

(A color version of this figure is available in the online journal.)

(see bottom panel in Figure 5). Note that Neptune's eccentricity never becomes large in this simulation ($e_{\rm N} < 0.03$). This kind of simulation thus clearly satisfies the CC constraint discussed in Dawson & Murray-Clay (2012).

To study how HCs can be captured for this kind of evolution, we repeated the simulation with increased resolution. This is because the original number of disk particles was insufficient to obtain reasonable statistics on HC formation. First, we repeated the original runs, using the same initial conditions for planets and planetesimals, and recording the planetary orbits at one year time intervals. We then perform a second integration with our modified version of the `swift_rmvs3` integrator (Levison & Duncan 1994), where the planetary orbits are read from the file recorded above and are interpolated to the required sub sampling (generally 0.5 yr, which is the integration time step used here). The interpolation was done in Cartesian coordinates (Nesvorný et al. 2013). This assures that the orbital evolution of planets in these new integrations is practically the same (up to small errors caused by the interpolation routine) as in the original runs. The new simulations included 70,000 disk particles with orbits respecting the original distribution of disk particles (i.e., 23 AU $< a <$ 30 AU, zero eccentricities and zero inclinations).

Figure 6 shows an example of a particle that eventually reaches the HC orbit with $a = 42$ AU, $e = 0.08$, and $i = 17°$. Its evolution is reminiscent of the two cases discussed for Model A above. The particle is captured in a 3:5 resonance with Neptune at $t \simeq 2 \times 10^7$ yr, and although it is difficult to see on the scale of the upper panel in Figure 6, it is actually released from the

resonance at $t \simeq 8 \times 10^7$ yr. The Kozai oscillations are readily seen for 25 Myr $< t <$ 60 Myr, while the particle is still in 3:5 MMR. Due to these oscillations, the particle is capable of reaching a relatively large perihelion distance, decouples from Neptune, and once it is released from the MMR, it ends up in the middle of the HC population.

By analyzing all of the particles that ended on an HC orbit in our Model B, we found that ~80% of them followed the path of particle illustrated above, but also involving other resonances, such as the 4:7 MMR. The final orbital distribution of these particles is very similar to that shown in Figure 2, and represents a good match to the orbital distribution of real HCs. (We do not claim that the match is good in any formal statistical sense because we have not obtained enough HC particles for a statistical test to be meaningful. A more careful comparison will require increased resolution and will be done in future.)

We therefore find that the mechanism discussed in Section 2 is not limited to a case with high-eccentricity evolution of Neptune, but also applies to a case where Neptune's eccentricity remains low. This is useful because it shows that the mechanism advocated here is not in contradiction to the CC constraint (Dawson & Murray-Clay 2012). Moreover, this shows that the HC population need not necessarily be formed by the secular mechanism suggested by Dawson & Murray-Clay (2012) which requires a high-eccentricity phase of Neptune. Instead, even if Neptune's eccentricity stays low, HCs can still form by the mechanism discussed here. The efficiency of our mechanism and how it depends on Neptune's eccentricity is discussed in Section 5.

This is both good and bad news. The bad news is that the HC constraint discussed in Dawson & Murray-Clay (2012) does not necessarily apply, because it was devised for a different mechanism. The good news is that the constraints from the CCs and HCs are not as contradictory as they otherwise would be (see Figure 20 in Dawson & Murray-Clay 2012), because the migration models with $e_N \lesssim 0.15$ should satisfy both.

4. MODEL C: INCREASED RESOLUTION BETWEEN 41 AND 46 AU

We have performed this additional set of simulations to investigate the effect of relatively weak MMRs in the HC region, such as the 4:7, 5:9, 6:11, 7:12, and 7:13 MMRs. We wanted to see whether the mode of behavior discussed in previous sections can also occur for these weak resonances. In addition, we increased the temporal sampling of orbital evolution in these new simulations such that we can see, in detail, the behavior of resonant angles. On the downside, these simulations do not globally follow the orbital evolution of particles from before the instability. Instead, we only track the orbital evolution of particles from the scattered disk, and follow the slow residual migration of Neptune. This is done as follows.

In the first step, we consider a heliocentric system with Jupiter, Saturn, and Uranus initially having the orbital elements for Julian date 2454200.5, referred to as the ecliptic plane. In nine different simulations, Neptune is placed in an orbit with a semi-major axis in the range 29.66 AU $\leqslant a_N \leqslant$ 30.06 AU with individual values placed $\Delta a = 0.05$ AU apart in different runs. Other orbital elements of Neptune were also taken on Julian date 2454200.5. Note, therefore, that the eccentricity of Neptune is small initially (mean ≃0.01) and remains low during the integration.

We also consider in each simulation a disk of 5000 massless scattered particles ranging from $a \sim 41$ AU to $a \sim 46.4$ AU with $0 < i \leqslant 50^\circ$, $a_N < q \leqslant 35$ AU, and the orbital angles ω, nodal longitude Ω, and mean anomaly l randomly distributed between 0° and 360°. The simulations in this first step were performed up to 2 Gyr with non-migrating Neptune (as the planetesimals are massless and no artificial migration was induced). The scattered disk objects are trapped into resonances or scattered away during this phase.

In the second step, we have taken the end results of step 1 simulations, and forced Neptune to artificially migrate to its current semi-major axis. This was done by including a velocity-dependent force into Neptune's equations of motion. The speed of Neptune's migration was set to be $da/dt = 0.5$ AU Gyr^{-1}, as this is roughly the speed measured after the scattering event in Model A. The simulations of the second step were stopped when Neptune's semi-major axis reached its current mean value. Below, we discuss two examples taken from these simulations.

The first example is shown in Figure 7 where a scattered particle is captured by the 3:5 MMR (see the resonant angle in the bottom right panel). Once the particle is trapped in an MMR, the Kozai resonance can appear even for relatively small inclinations (Gallardo et al. 2012). In the case shown in Figure 7, the Kozai oscillations occur for $i \sim 10^\circ$ starting at $t \simeq 250$ Myr. This makes the particle's perihelion distance and inclination (bottom left panel) pass through large variations for up to 1.2 Gyr, when both Kozai and 3:5 MMR variations temporarily disappear (see the right top and bottom panels). The orbit is fairly stable, with $q > 35$ AU for more than 300 Myr. This behavior resembles the so-called hibernating mode discussed in Gomes (2011). However, as Neptune is still not migrating at this time, the resonances become active again (between 1.5 Gyr and 1.7 Gyr, and after 1.85 Gyr). When Neptune starts to migrate at 2 Gyr, the particle orbit follows Neptune's migration, as can be seen in the top left panel. Then, at ≃2.25 Gyr, it dynamically "hibernates" during a stage when both resonant angles librate with very high amplitudes and the perihelion distance stays $q > 36$ AU for a long period. The orbit continues to migrate, but at 2.7 Gyr it stops as it is released from the 3:5 MMR, and ends up on a stable HC orbit with $e \simeq 0.1$ and $i \simeq 12^\circ$.

Compared to the example with 3:5 MMR discussed in the previous section (Figure 6), the resolution is significantly better, which allows us to see in more detail the behavior of the resonant angles. For example, it is possible to identify a relatively uncommon mode of the Kozai resonance where the center of liberations occurs at $\omega = 0$ at $t \simeq 400$ Myr or $\omega = 180^\circ$ at $t \simeq 500$ Myr. It is also clear that the critical angle of the 3:5 MMR librates with a very high amplitude (≃100°) during the time of Kozai oscillations.

Another example is shown in Figure 8. In this case, the particle is captured in 4:7 MMR. The libration of the Kozai angle occurs around more standard values $\omega = 90^\circ$ and $\omega = 270^\circ$. This shows that inside different MMRs, the stable equilibrium points of the Kozai resonance can be different. Once the particle reaches the Kozai resonance, high variations of orbital eccentricity and perihelion distance are again noted. The hibernation mode can be identified between 400 Myr and 500 Myr and between 1.4 Gyr and 1.42 Gyr. From 1 to 1.25 Gyr the object experiences a phase during which its perihelion distance is close to Neptune (32 AU $< q <$ 36 AU). Close encounters with the planet are avoided, however, because of the phase-protection mechanism provided by the 4:7 MMR. Once the residual migration is included, at $t = 2$ Gyr, the Kozai and

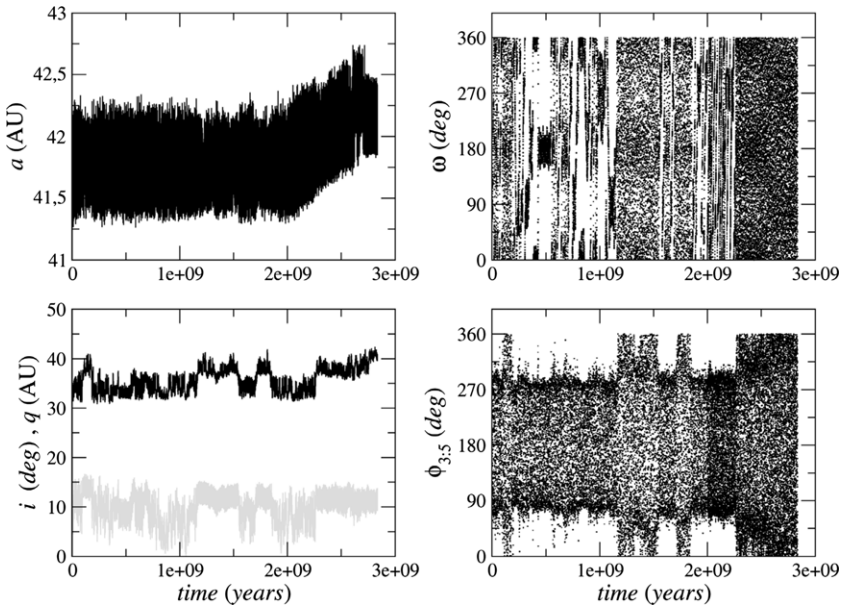

Figure 7. Orbital evolution of a particle from Model C. We show its semi-major axis in the top left panel, perihelion distance (black), and inclination (gray) in the bottom left panel, argument of perihelion, ω, in the top right panel, and 3:5 MMR angle in the bottom right panel. The system remains "static" for up to 2 Gyr when we initiate Neptune's residual migration. The particle is eventually released on a stable HC orbit with $q \simeq 40$ AU and $i \simeq 12^\circ$.

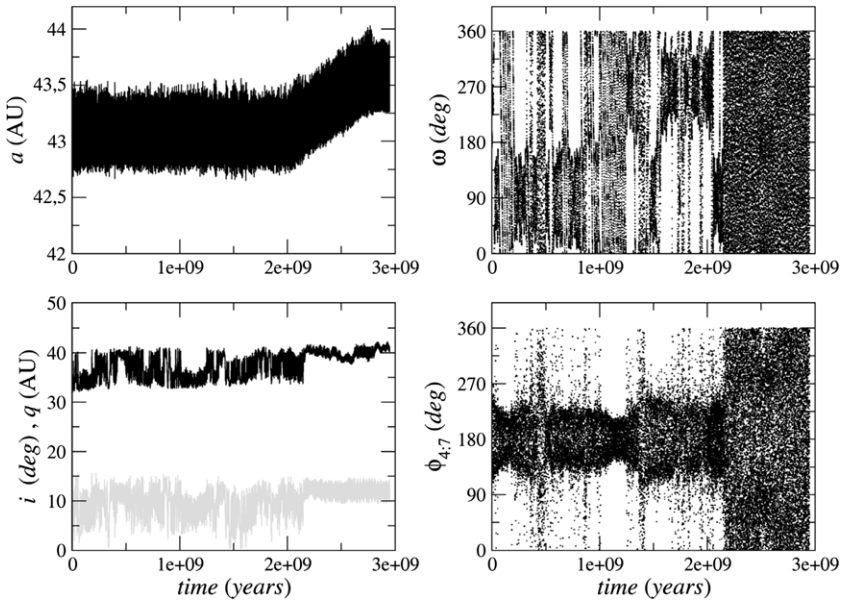

Figure 8. Same as Figure 7, but for a particle first trapped by the 4:7 MMR. The particle reached an HC orbit with $q \simeq 41$ AU and $i \sim 12^\circ$ after being released from the resonance.

4:7 resonances persist for additional $\simeq$200 Myr. Finally, the particle is released from the MMR at $t = 2.8$ Gyr. The result is an HC orbit with $a = 43.5$ AU, $e = 0.06$, and $i = 12^\circ$.

In addition to the examples discussed above, we also identified numerous cases of particles that show the same type of behavior in even weaker resonances, such as the 6:11, 7:12, and 7:13 MMRs. We therefore conclude that the weak resonances are capable, at least in principle, of lifting orbits from the scattered disk and transport them into the HC region. The expected result is that the HC orbits created by this process should populate the whole region of the HCs with a distribution that does not show a strong tendency toward the semi-major axis location of strong MMRs. This explains why the semi-major axis distribution of HCs in Figure 2 nearly uniformly covers 41–47 AU.

5. DISCUSSION AND CONCLUSIONS

We demonstrated a new mechanism for the dynamical origin of orbits in the HC population. Using different scenarios for the early evolution of Neptune's orbit, motivated by modern theories, we showed that the HC orbits are reached by the following process.

1. A planetesimal is scattered by Neptune, or another giant planet, during the planetary instability.
2. While on an orbit in Neptune's scattered disk, the planetesimal is trapped in an exterior MMR with the migrating Neptune.
3. After being trapped with large libration amplitude in the MMR, the Kozai resonance, which is present in MMRs even

for moderate inclinations (Gallardo et al. 2012), becomes important.

4. The Kozai resonance decreases the orbital eccentricity of the planetesimal, which leads to an orbit that is decoupled from Neptune.
5. While Neptune is still migrating, the planetesimal's orbit falls off of the MMR and becomes "fossilized" with relatively low eccentricity and significant inclination.

Here, we illustrated this process in detail for the 1:2, 3:5, 4:7, and 5:9 MMRs with Neptune and determined that it occurs in even weaker resonances, such as the 6:11, 7:12, and 7:13 MMRs. In addition, using two different models of Neptune's orbital evolution, we demonstrated that the process occurs independently of the detailed evolution of Neptune's eccentricity. The orbital distribution of HC particles produced in our simulations bears a close resemblance to that of real HCs. Taken together, we believe that this mechanism is robust and potentially of crucial importance for the formation of the Kuiper Belt. Note that the general significance of this mechanism was first pointed out in Gomes (2003a, 2003b), where it was studied in the context of a model with smooth migration of Neptune. Also, see Gomes (2011) and Brasil et al. (2014) for the application of this mechanism to the extended scattered disk.

We find that the probability of capture in an HC orbit ($i > 5°$, $q > 30$ AU, and 40 AU $< a <$ 47.5 AU) for each particle in the primordial disk is $50/60{,}000 \simeq 10^{-3}$ in our Model A and $6/70{,}000 \simeq 10^{-4}$ in Model B. With the original disk mass $M_{\rm disk} = 42\ M_{\rm Earth}$, Model A would imply a mass of the HC population of $M_{\rm HC} = 0.04\ M_{\rm Earth}$. Model B, with $M_{\rm disk} = 20\ M_{\rm Earth}$, instead, would imply a much lower mass of $M_{\rm HC} = 0.002\ M_{\rm Earth}$.

This large contrast between the predictions of Models A and B, besides being of different disk masses used in these models, is likely caused by different values of eccentricity reached by Neptune in the aftermath of planetary instability (0.4 in Model A and 0.025 in Model B), mainly because the capture probability in MMRs, and the efficiency of the whole mechanism advocated here, should increase with larger values of $e_{\rm N}$ (i.e., resonances become wider and stickier with larger $e_{\rm N}$). A detailed analysis of this issue goes beyond the scope of the work presented here. In addition, the larger capture probability in Model A is related to the fact that the initial planetesimal disk extended all the way to 40 AU. It is easier to implant bodies into the HC orbits if they start at 30–40 AU than if they start below 30 AU as in Model B.

For comparison, Fraser et al. (2014) estimated that the mass of HCs between the 2:3 and 1:2 MMRs is 0.005 $M_{\rm Earth}$ (∼50% uncertainty). Interpreted in the context of our simulations, this could mean that the largest eccentricity value attained by Neptune was somewhat intermediate between our two extreme cases, speculatively near 0.1.

As a final note, we would like to point out that while we believe that the mechanism discussed here plays an important role in the dynamical formation of the Kuiper Belt, it is likely that the complex structures seen in the trans-Neptunian region are contributed by many different dynamical processes. Clearly, the scope of our work is not to address the dynamical formation of Plutinos in 2:3 resonance or that of the CCs. Instead, we just want to point out a dynamical mechanism that can be important for the HCs (and the extended scattered disk; Gomes 2011). Additional work will be needed to develop a definitive global model of the Kuiper Belt origin, and to see if different constraints can be simultaneously met.

P.I.O.B. acknowledges supports from FAPESP (grants 2011/08540-9 & 2012/23719-8), R.S.G. thanks CNPq for grant 301878/2007-2, and D.N. acknowledges support from the NASA OPR program.

APPENDIX

NM12 INSTABILITY MODELS

Nesvorný & Morbidelli (2012, hereafter NM12) reported the results of a statistical study in which they performed nearly 10^4 numerical simulations of planetary instability starting from hundreds of different initial conditions. Here, we briefly describe the initial conditions and success criteria used in NM12. Our goal is to justify Model B discussed in the main text, which was based on the NM12 simulations.

In the first step (Phase 1), NM12 performed hydrodynamic and *N*-body simulations to identify the resonant configurations which may have occurred among the young solar system's giant planets. The planets with masses corresponding to those of Jupiter, Saturn, and ice giants, ordered in increasing orbital distance from the Sun, were placed on initial orbits with period ratios slightly larger than those of the selected resonances, and were then migrated into resonances (to mimic the convergent gas-driven migration of orbits). NM12 considered cases with four, five, and six initial planets where the additional planets were placed onto resonant orbits between Saturn and the inner ice giant, or beyond the orbit of the outer ice giant. Additional planets were given the mass between one-third and three times the mass of Uranus.

Different starting positions of planets, rates of the semi-major axis and eccentricity evolution (as implied by different gas disk densities), and timescales for the gas disk's dispersal produced different results. For Jupiter and Saturn, NM12 confined the scope of their study to the 3:2 and 2:1 resonances because the former is strongly preferred from previous hydrodynamic studies (e.g., Masset & Snellgrove 2001). The 2:1 resonance was included as a reference case.

In Phase 2 of their study, NM12 tracked the evolution of planetary orbits through and past the instability. These simulations included the effects of the transplanetary planetesimal disk. The planetesimals were placed onto initial orbits with low orbital eccentricities and inclinations. The outer edge of the disk was placed at $r_{\rm out} = 30$ AU, such that the planetesimal-driven migration parked Neptune near its present semi-major axis. NM12 considered different masses of the planetesimal disk, $M_{\rm disk}$, with $M_{\rm disk}$ between 10 and 100 $M_{\rm Earth}$. Thirty simulations were performed in each case, where different evolution histories were generated by randomly seeding the initial orbit distribution of planetesimals. The number of simulations was increased to 100 in the interesting cases. In total, NM12 completed nearly 10^4 scattering simulations from over 200 different initial states. Each system was followed for 100 Myr with the standard *SyMBA* integrator (Duncan et al. 1998).

NM12 defined four criteria to measure the overall success of their simulations. First of all, the final planetary system must have four giant planets (criterion A) with orbits that resemble the present ones (criterion B). Note that A means that one and two planets must be ejected in the five- and six-planet cases, while all four planets need to survive in the four-planet case. As for B, NM12 claimed success if the final mean semi-major axis of each planet was within 20% of its present value, and if the final mean eccentricities and mean inclinations were no larger than $0.^{\circ}11$ and $2°$, respectively. For the successful runs,

as defined above, NM12 also checked the history of encounters between giant planets, the evolution of the secular g_5, g_6, and s_6 modes, and the secular structure of the final planetary systems. They required that $e_{55} > 0.022$ in the final systems, where e_{55} is the amplitude of the fifth eccentric mode in Jupiter's orbit (i.e., at least half of its current value; criterion C). Finally, criterion D was used in NM12 to account for the terrestrial planets and asteroid belt.

NM12 found that the initially compact resonant configurations and low masses of the planetesimal disk ($M_{\rm disk} < 50$ $M_{\rm Earth}$) typically lead to violent instabilities and planet ejection. On the other hand, the initial states with orbits that are more radially spread out (e.g., Jupiter and Saturn in the 2:1 resonance) and larger $M_{\rm disk}$ were found to result in smooth migration of the planetary orbits which leads to incorrectly low e_{55} and excitation of the terrestrial planet orbits. Finding the sweet spot between these two extremes was difficult.

Some of the statistically best results were obtained in NM12 when assuming that the solar system initially had five giant planets and one ice giant, with a mass comparable to that of Uranus and Neptune, was ejected into interstellar space by Jupiter. The best results were obtained when the fifth planet was assumed to have a mass similar to Uranus/Neptune, was placed on an orbit just exterior to Saturn's (3:2 and 4:3 resonances work best), and the orbits of Uranus and Neptune migrated into the planetesimal disk before the onset of planetary scattering. This mode of instability was favored for several reasons, as described below.

As planetesimals are scattered by Uranus and Neptune and evolve into the Jupiter/Saturn region, Jupiter, Saturn, and the fifth planet undergo divergent migration. This triggers an instability during which the fifth planet suffers close encounters with all planets and is eventually ejected from the solar system by Jupiter. Uranus and Neptune generally survive the scattering phase because their orbits migrated outward during the previous stage and opened a protective gap between them and the gas giants. This mode of instability produces just the right kind of Jupiter's semi-major axis evolution—known as jumping Jupiter—that is required from the terrestrial planet constraint.

Moreover, e_{55}, excited by the fifth planet ejection, is not damped to incorrectly low values by secular friction from the planetesimal disk because the planetesimal disk had been disrupted by Uranus and Neptune before the excitation event. The low mass of the planetesimal disk at the time of planet scattering also leads to only a brief migration phase of Jupiter and Saturn after the scattering phase, and prevents $P_{\rm Sat}/P_{\rm Jup}$ from evolving beyond its current value. The excessive residual migration of Jupiter and Saturn was a problem in most other cases investigated in NM12.

Our initial setup for Model B described in the main text closely follows the setup of the most successful models described in NM12. We used a slightly larger semi-major axis of Uranus than in NM12 to avoid a problem with NM12 simulations where Uranus and Neptune frequently migrated past their 2:1 resonance (while they did not in the real solar system). With this slight adjustment, the results of instability simulations are applicable to the Kuiper Belt, which is the main focus here.

REFERENCES

Batygin, K., Brown, M. E., & Betts, H. 2012, ApJL, 744, L3
Batygin, K., Brown, M. E., & Fraser, W. C. 2011, ApJ, 738, 13
Bernstein, G. M., Trilling, D. E., Allen, R. L., et al. 2004, AJ, 128, 1364
Brasil, P. I. O., Gomes, R. S., & Soares, J. S. 2014, A&A, 564, A44
Brasser, R., Morbidelli, A., Gomes, R., Tsiganis, K., & Levison, H. F. 2009, A&A, 507, 1053
Brown, M. E. 2001, AJ, 121, 2804
Chambers, J. E. 1999, MNRAS, 304, 793
Dawson, R. I., & Murray-Clay, R. 2012, ApJ, 750, 43
Duncan, M. J., & Levison, H. F. 1997, Sci, 276, 1670
Duncan, M. J., Levison, H. F., & Lee, M. H. 1998, AJ, 116, 2067
Edgeworth, K. E. 1949, MNRAS, 109, 600
Fernandez, J. A., & Ip, W.-H. 1984, Icar, 58, 109
Fraser, W., Brown, M. E., Morbidelli, A., Parker, A., & Batygin, K. 2014, ApJ, 783, 100
Gallardo, T., Hugo, G., & Pais, P. 2012, Icar, 220, 392
Gladman, B., Holman, M., Grav, T., et al. 2002, Icar, 157, 269
Gomes, R. 2003a, EM&P, 92, 29
Gomes, R., Levison, H. F., Tsiganis, K., & Morbidelli, A. 2005a, Natur, 435, 466
Gomes, R. S. 2000, AJ, 120, 2695
Gomes, R. S. 2003b, Icar, 161, 404
Gomes, R. S. 2011, Icar, 215, 661
Gomes, R. S., Fernández, J. A., Gallardo, T., & Brunini, A. 2008, in The Solar System Beyond Neptune, ed. M. A. Barucci, H. Boehnhardt, D. P. Cruikshank, & A. Morbidelli (Tucson, AZ: Univ. Arizona Press), 259
Gomes, R. S., Gallardo, T., Fernández, J. A., & Brunini, A. 2005b, CeMDA, 91, 109
Hahn, J. M., & Malhotra, R. 2005, AJ, 130, 2392
Jewitt, D., & Luu, J. 1993, Natur, 362, 730
Jewitt, D., Luu, J., & Trujillo, C. 1998, AJ, 115, 2125
Kenyon, S. J., & Luu, J. X. 1999, AJ, 118, 1101
Kozai, Y. 1962, AJ, 67, 591
Kozai, Y. 1985, CeMec, 36, 47
Kuiper, G. P. 1951, PNAS, 37, 1
Kuiper, G. P. 1974, CeMec, 9, 321
Levison, H. F., & Duncan, M. J. 1994, Icar, 108, 18
Levison, H. F., & Morbidelli, A. 2003, Natur, 426, 419
Levison, H. F., Morbidelli, A., Van Laerhoven, C., Gomes, R., & Tsiganis, K. 2008, Icar, 196, 258
Levison, H. F., & Stern, S. A. 2001, AJ, 121, 1730
Malhotra, R. 1993, Natur, 365, 819
Malhotra, R. 1995, AJ, 110, 420
Malhotra, R. 1998, Lunar and Planetary Institute Science Conference Abstracts, 29, 1476
Masset, F., & Snellgrove, M. 2001, MNRAS, 320, L55
Morbidelli, A., Brasser, R., Gomes, R., Levison, H. F., & Tsiganis, K. 2010, AJ, 140, 1391
Morbidelli, A., Brasser, R., Tsiganis, K., Gomes, R., & Levison, H. F. 2009, A&A, 507, 1041
Morbidelli, A., Levison, H. F., Tsiganis, K., & Gomes, R. 2005, Natur, 435, 462
Morbidelli, A., & Valsecchi, G. B. 1997, Icar, 128, 464
Nesvorný, D. 2011, ApJL, 742, L22
Nesvorný, D., & Morbidelli, A. 2012, AJ, 144, 117
Nesvorný, D., Vokrouhlický, D., & Morbidelli, A. 2013, ApJ, 768, 45
Parker, A. H., & Kavelaars, J. J. 2010, ApJL, 722, L204
Petit, J.-M., Morbidelli, A., & Valsecchi, G. B. 1999, Icar, 141, 367
Tsiganis, K., Gomes, R., Morbidelli, A., & Levison, H. F. 2005, Natur, 435, 459